RESEARCH ARTICLE

Different protein expression patterns in rat spinal nerves during Wallerian degeneration assessed using isobaric tags for relative and absolute quantitation proteomics profiling

Shuai Wei[1, 2, 3, #], Xue-Zhen Liang[2, 4, #], Qian Hu[1, #], Wei-Shan Wang[1], Wen-Jing Xu[2], Xiao-Qing Cheng[2, 3], Jiang Peng[2, 3], Quan-Yi Guo[2], Shu-Yun Liu[2], Wen Jiang[1, 2, 3], Xiao Ding[1, 2, 3], Gong-Hai Han[2, 3, 5], Ping Liu[2, 3, 6], Chen-Hui Shi[1, *], Yu Wang[2, 3, *]

1 The First Affiliated Hospital of Medical College, Shihezi University, Shihezi, Xinjiang Uygur Autonomous Region, China
2 Institute of Orthopedics, Chinese PLA General Hospital, Beijing, China
3 Co-Innovation Center of Neuroregeneration, Nantong University, Nantong, Jiangsu Province, China
4 The First Clinical Medical School, Shandong University of Traditional Chinese Medicine, Jinan, Shandong Province, China
5 Kunming Medical University, Kunming, Yunnan Province, China
6 Shanxi Medical University, Taiyuan, Shanxi Province, China

Funding: *This study was supported by National Key Research & Development Program of China, No. 2016YFC11011601, 2017YFA0104701, the Youth Cultivation Project of Military Medical Science, China, No. 15QNP091 (to YW), and People's Liberation Army Youth Training Project for Medical Science of China, No. 16QNP144 (to YW).*

Graphical Abstract

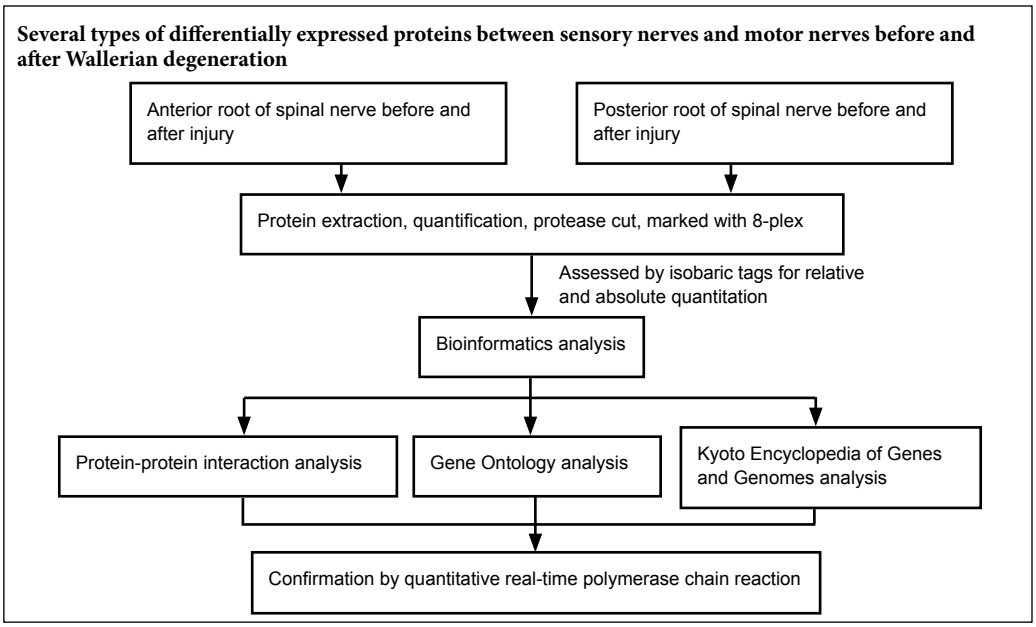

Correspondence to:
Yu Wang, MD, wangwangdian628@126.com; Chen-Hui Shi, 1512905535@qq.com.

 # These authors contributed equally to this paper.

orcid:
0000-0001-7811-5834 (Yu Wang)

doi: *10.4103/1673-5374.265556*

Received: *October 27, 2018*
Accepted: *March 4, 2019*

Abstract

Sensory and motor nerve fibers of peripheral nerves have different anatomies and regeneration functions after injury. To gain a clear understanding of the biological processes behind these differences, we used a labeling technique termed isobaric tags for relative and absolute quantitation to investigate the protein profiles of spinal nerve tissues from Sprague-Dawley rats. In response to Wallerian degeneration, a total of 626 proteins were screened in sensory nerves, of which 368 were upregulated and 258 were downregulated. In addition, 637 proteins were screened in motor nerves, of which 372 were upregulated and 265 were downregulated. All identified proteins were analyzed using the Gene Ontology and Kyoto Encyclopedia of Genes and Genomes analysis of bioinformatics, and the presence of several key proteins closely related to Wallerian degeneration were tested and verified using quantitative real-time polymerase chain reaction analyses. The differentially expressed proteins only identified in the sensory nerves were mainly relevant to various biological processes that included cell-cell adhesion, carbohydrate metabolic processes and cell adhesion, whereas differentially expressed proteins only identified in the motor nerves were mainly relevant to biological processes associated with the glycolytic process, cell redox homeostasis, and protein folding. In the aspect of the cellular component, the differentially expressed proteins in the sensory and motor nerves were commonly related to extracellular exosomes, the myelin sheath, and focal adhesion. According to the Kyoto Encyclopedia of Genes and Genomes, the differentially expressed proteins identified are primarily related to various types of metabolic pathways. In conclusion, the present study screened differentially expressed proteins to reveal more about the differences and similarities between sensory and motor nerves during Wallerian degeneration. The present findings could provide a reference point for a future investigation into the differences between sensory and motor nerves in Wallerian degeneration and the characteristics of peripheral nerve regeneration. The study was approved by the Ethics Committee of the Chinese PLA General Hospital, China (approval No. 2016-x9-07) in September 2016.

Key Words: *gene ontology; Kyoto Encyclopedia of Genes and Genomes; isobaric tags for relative and absolute quantitation; motor nerve; proteomics; sensory nerve; spinal nerve; Wallerian degeneration*

Chinese Library Classification No. *R446; R363; R741*

Introduction

Peripheral nerve injury often leads to limb dysfunction. In China, approximately 700,000 patients are surgically treated for peripheral nerve injury every year (Kearns and Wang, 2012). Following peripheral nerve injury, Wallerian degeneration (WD) takes place, and myelin sheath disintegration, axonal degradation, and inflammatory cell infiltration occur at the distal end of the injured axon (Chang et al., 2017; Bittner et al., 2018; Han et al., 2019). While nerve injury causes significant damage to nerve functions, it also plays an important role in peripheral nerve regeneration (Xiong et al., 2016; Caillaud et al., 2019). Wallerian degeneration is the innate immune response of peripheral nerve to injury, rapid removal of degenerated axons and debris of myelin sheath is beneficial to axon regeneration. Nerve injury differences between sensory and motor pathways have been identified in previous work; notably, motor axons withdraw from the skin in a wrong pathway and re-control the appropriate muscle that they belong to (Langley and Anderson, 1904; Ramon y Cajal, 1928). Thus, compared with the skin branches, motor neurons of the femoral nerve can be in a dominant position of muscle branches after transection, even if they have the chance to reach skin branches (Brushart, 1988). There are inherent differences between motor nerve (MN) and sensory nerve (SN) fibers in peripheral nerves, and studies have revealed that these differences play an important role in nerve fiber regeneration during WD (Abdullah et al., 2013).

There are many animal models of peripheral nerve injury, which are most commonly used to study the sciatic and femoral nerves (Cobianchi et al., 2014; Ding et al., 2015; Karegar and Mohammadi, 2015). Some researchers have found that the muscular branch of femoral nerve mainly contains motor nerve fibers, while the cutaneous branch of femoral nerve mainly contains sensory nerve fibers. Because of the purity of muscular and cutaneous nerve branches in femoral nerves, they are often used to study chemotactic regeneration of the peripheral nerve (Zhang et al., 2016; Cai et al., 2017). To improve functional recovery via peripheral nerve regeneration, it is important to have a full understanding of the essential biological differences between SNs and MNs (Raivich and Kreutzberg, 1993). Previous work has revealed that regenerating motor axons express a molecule called polysialylated, which is a form of the neural cell adhesion molecule (Franz et al., 2005, 2008). This suggests that sensory and motor neuron axons have different microenvironment regeneration strategies. However, most peripheral nerves are composed of both SNs and MNs, and it is difficult to find pure SNs or MNs; it is therefore a challenge to examine this hypothesis. To overcome this, most researchers investigate spinal nerves; the anterior and posterior roots of spinal nerves are pure SNs and MNs, respectively, and can therefore be used to exclude the influence of mixed nerve branches, and are therefore ideal for studying different regenerating microenvironments of SNs and MNs.

The standard method used for proteomic analysis is two-dimensional electrophoresis followed by MS (mass spec-trometry)-based protein identification (López-Barea and Gómez-Ariza, 2006). This proteomics strategy is a useful method for the comprehensive study of multiple proteins in many tissues (Becker et al., 2008; Lu et al., 2009). Isobaric tags for relative and absolute quantitation (iTRAQ) is a powerful proteomics labeling technique that can be used for quantitating multiple specimens in a single MS run (Unwin et al., 2010). Therefore, the present study used iTRAQ to compare the protein profiles of spinal nerves after injury, and focused on the four following tissue types: pure SNs and MNs in spinal sections from rats before and after injury. The present findings will provide a reference point that will allow future studies to identify differences in WD in MNs and SNs, and better characterize peripheral nerve regeneration.

Materials and methods

Tissue collection

Sixty 8-week-old male adult specific-pathogen-free Sprague-Dawley (SD) rats, weighing 200–250 g, were anesthetized by intraperitoneal injection of moderate sodium pentobarbital (Xingzhi Chemical Plant, Shanghai, China) (30 mg/mL, 30 mg/kg) prior to surgery. After tissue collection, rats received an overdose of sodium pentobarbital to euthanasia (30 mg/mL, 0.6 mL). Twenty rats were used in quantitative real-time polymerase chain reaction (qRT-PCR) experiments and forty rats were used in the proteomic analysis. The L2 posterior root nerve and anterior root nerve were transected on the right side. The left side was used as the control. One week later, tissues of the distal stump of the injured L2 posterior root nerve and the proximal stump of the injured L2 anterior root nerve were obtained as the experimental group; the normal L2 posterior root nerve and anterior root nerve were obtained as a control group. There were eight samples in total, which included two from each group. The experimental procedure related to experimental animals were approved by the Ethics Committee of the Chinese PLA General Hospital, China (Approval No. 2016-x9-07) in September 2016. All procedures with experimental animals were performed in accordance with the Guides for the Care and Use of Laboratory Animals. The rats used in this study were raised in a sterile environment and provided by the Laboratory Animal Research Center of The First Clinical Center, Chinese PLA General Hospital (license No. SCXK (Jing) 2016-0002).

Specimen preparation

After the specimens had been obtained, they were quickly placed in cryotubes and stored in liquid nitrogen. Four tissue groups were examined, as follows: tissues of the distal stump of the injured L2 posterior root nerve formed the SN after injury (SI) group; tissues of the normal L2 posterior root nerve formed the normal SN group; tissues of the proximal

stump of the injured L2 anterior root nerve formed the MN after injury (MI) group; and tissues of the normal L2 anterior root nerve formed the normal MN group. All samples were dissolved by vortex mixing, adequately homogenized in 1 mL of lysis buffer, and then disposed by the sonicate (Xu et al., 2017) at 120 W for 60 seconds, which was conducted on an ice-water mixture. The supernatant was collected and stored after ultrasonic extraction and centrifuged for 20 minutes. Then, the concentrations of proteins were measured using the Bradford method (Bradford, 1976).

Isobaric tags for relative and absolute quantitation labeling and liquid chromatography-mass spectrometer/mass spectrometer analysis

On the basis of the specification requirements, compound samples were extracted, then labeled using the iTRAQ Reagent-8plex Multiplex Kit (PN:4390812; AB SCIEX, Framingham, MA, USA). The SN samples were labeled with iTRAQ tags 113 and 114, and the SI samples were labeled with tags 115 and 116; the MN samples were labeled with iTRAQ tags 117 and 118, and the MI samples were labeled with tags 119 and 121. Later, the total peptides labeled with iTRAQ tags were mixed at equal proportions, then decomposed with high pH C18 chromatography, and 12 fractions were obtained. Finally, the total fractions were analyzed by liquid chromatography-MS and separated by an AB SCIEX system with a buffer composed of buffer A (0.1% formic acid and 5% acetonitrile), buffer B (95% acetonitrile and 0.1% formic acid), and a loading buffer (0.1% formic acid and 3% acetonitrile). The MS equipment comprised an AB SCIEX analytical column, a new objective needle, and a Chromxp Trap Column.

Analysis of differentially expressed proteins

To identify the main functional pathways of the differentially expressed proteins (DEPs) in injured nerves, the Gene Ontology (GO) and Kyoto Encyclopedia of Genes and Genomes (KEGG) pathway-enrichment analyses were performed using the Database for Annotation, Visualization, and Integrated Discovery (DAVID) 6.8 (https://david.ncifcrf.gov/). The statistical threshold was set as $P < 0.05$ with fold change (FC) ≥ 1.5.

Protein-protein interaction networks construction and analysis

Based on the differentially expressed proteins identified in the previous step, we constructed a protein-protein interaction (PPI) network. For this, the search tool for the retrieval of interacting genes (STRING, version 10.5, https://string-db.org/) database was used; DEP pairs with a combined score > 0.4 were identified. Only connected nodes were retained, and Cytoscape (version 3.6.1, https://cytoscape.org/) was used to create a visualization of the network. The topological properties of every connected node in the PPI network were assessed using Network Analyzer, which revealed the topological significance of each connected node. The greater the quantitative value of the node, the greater its importance in the network.

Based on a previous study by Zhang et al. (2013), significant targets were defined as nodes, of which the degrees were more than twice that of the median degree in all nodes. To explore the molecular complexes and the specific regulatory relationships between proteins in the PPI network, module analysis of the network was conducted using MCODE1.5.1 (https://cytoscape.org/), which is a plugin for Cytoscape (Halary et al., 2010) that calculates node information such as neighbors and density for each node in the network graph. It then builds functional modules for clustering using K-Core analysis. Data parameters were set with applicable thresholds of K-Core > 5.

Gene Ontology and Kyoto Encyclopedia of Genes and Genomes analyses

The DAVID database provides a comprehensive set of functional annotation, visualization, and integrated discovery tools (Huang da et al., 2009) to allow researchers to understand the biological implications of a large list of genes. It can be used to perform typical batch annotation and GO terminology-rich analyses to identify the related term of GO that have a close relationship with the gene list. The actual edition includes more than 40 categories, including GO terminology, PPI, general sequence characteristics, homology, gene function summaries, gene organization expression, and literature. GO enrichment and KEGG analyses of the above key differential genes were performed using the DA-VID 6.8 online analysis tool, and the R language ggplot2 installation package was used to draw bubble charts.

Quantitative real-time polymerase chain reaction

The total RNA was extracted from nerve tissues with TRIzol reagent (Thermo Fisher Scientific, Waltham, MA, USA). Every RNA sample was reverse transcribed into cDNA with a reverse transcription kit (TaKaRa, Tokyo, Japan) to detect mRNA, then qRT-PCR was used to quantify mRNAs levels. Glyceraldehyde-3-phosphate dehydrogenase was set as an internal reference. Detailed information about all primers is shown in **Table 1**.

Statistical analysis

The data are shown as the mean ± SD. Between-group differences were analyzed using a two-sample *t*-test and this analysis was performed using SPSS 22.0 (IBM, Armonk, NY, USA). The qRT-PCR results were shown by a histogram and created using GraphPad Prism 6.0 (GraphPad Software Inc., San Diego, CA, USA). Statistical significance was set at $P < 0.05$.

Results

Identification of proteins different with expression in the four sample types

A total of 626 proteins that were differentially expressed in both SN and SI groups were identified, of which 368 were upregulated and 258 were downregulated in response to the ratio of SN/SI. A total of 637 proteins that were differentially expressed in both MN and MI groups were identified, of which 372 were upregulated and 265 were downregulated in response to the ratio of MN/MI. All different proteins identified in the SN, SI, MN, and MI groups that were up- and down-regulated are shown in a heatmap (**Additional Figure 1**).

Table 1 Sequences of primers used for quantitative real-time polymerase chain reaction

Gene ID	Official name	Primer ID	Sequence (5′–3′)
24185	*Akt1*	Akt1-rat-F	ACCTCTGAGACCGACACCAG
		Akt1-rat-R	AGGAGAACTGGGGAAAGTGC
25012	*Snap25*	Snap25-rat-F	ACAGGATCATGGAGAAGG
		Snap25-rat-R	TTCCCAGCATCTTTGTTG
24520	*Kcna1*	Kcna1-rat-F	CATCCGCTTGGTAAGGGTGT
		Kcna1-rat-R	GGGGATACTGGAGAAGTGCG
117550	*Kif5b*	Kif5b-rat-F	ATGTAAAGCAACCGGAGGGG
		Kif5b-rat-R	CTGTTTGCAGCGTTTCACCA
84008	*Cntnap1*	Cntnap1-rat-F	CTCCGCATGATGAGTCTCCG
		Cntnap1-rat-R	CCATCCACTGATGCCGTGTAG
170673	*Palm*	Palm-rat-F	AGCAAGCGGAGACAATTGGA
		Palm-rat-R	TCTCGAGTCTGGTGATGGACT

Protein-protein interaction networks

By confluence different proteins using a composite score > 0.4, we constructed a network of PPI for the SN and SI groups using the STRING database. The network included 581 nodes (different proteins) and 4012 edges, which ac-counted for 92.81% of all proteins. For the MN and MI groups, the PPI network included 492 nodes (different proteins) and 3450 edges, which accounted for 77.24% of all proteins. The PPI networks were visualized in Cytoscape, through which relevant nodes were chosen for thorough analysis, and several irrelevant nodes were discarded. The resulting refined networks contained 358 nodes and 2446 edges for the SN and SI groups, and 443 nodes and 3450 edges for MN and MI groups. To analyze and process the large networks conveniently, they were extracted from the whole network. Based on a related study by Zhang et al. (2013), the specific nodes of all nodes of the SN and SI groups and 443 nodes of MN and MI groups were identified, of which the degrees were more than twice the median degree in all nodes. Thus, a network of candidate targets was constructed for SN and SI groups that had 87 nodes and 1067 edges, including 42 upregulated and 45 downregulated proteins (**Figure 1**). The network of candidate targets for the MN and MI groups had 131 nodes and 1768 edges, including 78 upregulated and 53 downregulated proteins (**Figure 2**).

Biological networks consist of various functional parts, which may be involved in biological processes of acquaintance. Hence, we created a new perspective on the biological function of complex networks. Using the MCODE analysis with a K-Core > 5, two were modules extracted from the PPI network. For the SN and SI network, one identified cluster included 30 nodes and 234 edges (cluster rank 1; K-Core 16.138), and the other included 26 nodes and 108 edges (cluster rank 2; K-Core 8.640; **Figure 3A** & **B**). For the MN and MI network, one identified cluster consisted of 24 nodes and 202 edges (cluster rank 1; K-Core 17.565), and the other consisted of 26 nodes and 165 edges (cluster rank 2; K-Core 13.200; **Figure 3C** & **D**).

Gene Ontology and Kyoto Encyclopedia of Genes and Genomes pathway analysis of functional patters of different genes

To reveal more specific functional patterns of these genes correspond to differently expressed proteins, 286 biological process items, 167 cellular component items, 124 molecular function items, and 57 KEGG signaling pathway items of SN and SI groups were obtained by introducing key differentially expressed genes into the DAVID online data tool for functional enrichment and pathway analysis; the top 10 significant *P*-values are presented as a bubble diagram (**Figure 4**). For the MN and MI groups, 65 biological process items, 42 cellular component items, 26 molecular function items, and 57 KEGG signaling pathway items were obtained; the top 10 *P*-values are presented as a bubble diagram (**Figure 5**). The results were divided into the two following parts: molecular functions/cellular components/biological processes and the KEGG pathway. In the SN and SI network, differentially expressed genes linked to biological processes were mainly related to cell-cell adhesion, carbohydrate metabolic processes, cell adhesion, and aging (**Figure 4A**); cellular components were mainly related to extracellular exosomes, myelin sheath, membrane, and cytoplasm (**Figure 4B**); molecular functions were mainly related to protein binding, cadherin binding involved in cell-cell adhesion, poly(A) RNA binding, and actin filament binding (**Figure 4C**); and the KEGG pathway was mainly related to antibiotic biosynthesis, carbon metabolism, amino acid biosynthesis, and protein processing in the endoplasmic reticulum (ER; **Figure 4D**). For the MN and MI network, the identified cellular components were mainly related to the presence of extracellular exosomes and myelin sheath, focal adhesion, and cytosol (**Figure 5A**); molecular functions were mainly related to poly(A) RNA binding, adenosine triphosphate (ATP) binding, protein disulfide isomerase activity, and GTPase activity (**Figure 5B**); biological processes were mainly related to glycolytic process, cell redox homeostasis, protein folding, and citrate metabolic processes (**Figure 5C**); and the KEGG pathway was mainly related to carbon metabolism, antibiotic biosynthesis, glycolysis/gluconeogenesis, and amino acid biosynthesis (**Figure 5D**).

Quantitative real-time polymerase chain reaction verified the expressions of key genes

The expressions of key genes in the SN, MN, SI, and MI tissues were measured using qRT-PCR. The expression of Akt1 was upregulated in SI samples compared with SN samples (MI *vs*. MN, $P = 0.0481$; SI *vs*. SN, $P < 0.0001$). However, the expression of Snap25 (MI *vs*. MN, $P < 0.0001$; SI *vs*. SN, $P < 0.0001$), Kcna1 (MI *vs*. MN, $P < 0.0001$; SI *vs*. SN, $P = 0.0004$), Kif5b (MI *vs*. MN, $P = 0.001$; SI *vs*. SN, $P = 0.0001$), Cntnap1 (MI *vs*. MN, $P = 0.0131$; SI *vs*. SN, $P = 0.0553$), and Palm (MI *vs*. MN, $P < 0.0001$; SI *vs*. SN, $P < 0.0001$) was lower in SI tissues than SN (**Figure 6**). The same genes were differentially expressed between MN and MI, with the same expression patterns. These results suggest that these genes may be involved in the injury process of sensory and motor nerves.

Discussion

Peripheral nerve injury can have adverse effects which can prolong the recovery time of injured nerves and affect the function of limbs, when nerve fibers become wrongly connected. Although some progress has been made toward treating peripheral nerve injury, such as tension reduction

suture of nerve stumps, autogenous nerve transplantation, and artificial nerve conduits, the clinical outcome remains unsatisfactory. Hence, it is urgent to clarify the mechanism of nerve injury to facilitate further treatment strategies for peripheral nerve injury. The present study revealed different protein expressions in the rat spinal nerve during WD using iTRAQ proteomics profiling and identified DEPs that could reveal differences and similarities between SNs and MNs during WD. The DEPs were correlated with a series of biological processes and pathways; the following discussion focuses on several types of DEPs found in SNs and MNs before and after injury.

Isobaric tags for relative and absolute quantitation analysis of the unique peptide

A unique peptide is one that is only present in one protein; detection of a unique peptide indicates the presence of the corresponding protein in a sample. The distribution of unique peptides shown a two-coordinate distribution curve of the number of unique peptides found in all proteins screened in this experiment (**Additional Figure 2**). A total of 3391 proteins contained at least two unique peptides, accounting for 78.64% of the total proteins. Each MS has its own measurement range and, thus, the identified peptides have certain length limitations. Therefore, if the peptide content detected by the MS used in the present study was too low or too high, the protease selection may have been inappropriate. The average polypeptide length was 13.6, which is within the reasonable range of peptide lengths (**Additional Figure 3**).

Key biological processes during Wallerian degeneration in sensory nerves

A total of 626 DEPs were screened in both SN and SI groups, of which 368 were upregulated and 258 were downregulated in response to WD. Results from the biological processes analysis, which identified the certain biological processes involved in the WD of SNs, along with those of the GO enrichment analysis suggested that these key genes are involved in cell-cell adhesion, carbohydrate metabolic processes, cell adhesion, aging, and protein folding.

Cell-cell adhesion and contact constitute fundamental physiological processes of multicellular organisms. Tissues are formed by different types of cells, and these cells must remain in physical contact with each other for structural and functional communications (Murakawa and Togashi, 2015). In the peripheral nervous system, the interactions between Schwann cells and axons also appear to be influenced by the deformation of Schwann cells in the microenvironment of injured and developing nerves (Namgung, 2014). In regenerating nerves, the guidance of the growth cone, axonal elongation, and myelination are correlated with the presence of Schwann cell and axon interaction (Pereira et al., 2012). The carbohydrate metabolic process could provide energy for many biological processes in tissues and could underlie different types of physiological activity, including WD. Many genes are involved in aging and, in the present study, Hspa8, which is the gene for the heat shock protein 70, had a higher expression level in SNs during WD compared to the normal nerve. Because of after its expression induced by ischemic stress, heat shock protein 70 may play a key role in protecting cells under mild stress conditions (Miller et al., 1991). Additionally, the unfolded or misfolded proteins in the ER accumulate as a result of multiple types of adverse stimulation, such as hypoxia, nutrient deprivation, and viral infection. Afterwards, the stress condition of the ER will be in turn triggered, and an evolutionarily conserved unfolded protein response will occur (Ron and Walter, 2007). In an animal model of optic nerve crush, in which most retinal ganglion cells are dead, Hu et al. (2012) demonstrated that the unfolded protein response was activated by axon injury in distinct pathways. In the present study, many genes were involved in the protein folding of biological processes, including *Cct3*, *Hspa*8, *Hspa*9, and *Hspa4l*. These findings may indicate that unfolded or misfolded proteins appear in injured nerve tissues during WD.

Key biological processes during Wallerian degeneration in motor nerves

A total of 637 DEPs were screened in both MN and MI groups, of which 372 were upregulated and 265 were down-regulated. The GO enrichment analysis suggested that these genes take part in the glycolytic process, cell redox ho-meostasis, and protein folding.

Much like the biological process of carbohydrate metabolism, the glycolytic process produces ATP for normal or abnormal physiological activities, including WD. In a study of the genesis of neuropathic pain, Lim et al. (2015) found increased oxygen consumption and lactate levels in the endoneurium in a mouse model of peripheral nerve injury, which suggests that the ATP levels in cells are maintained by anaerobic glycolysis. The changes of redox in cells plays a key part in the regulation of cell growth and aging, and have been reported to be correlated with a variety of neurodegenerative diseases (Kwon et al., 2003). In addition, because numerous signaling pathways within cells are sensitive to hypoxia conditions, altered intracellular redox plays an important role in the cell , such as cell homeostasis, cell proliferation and cell apoptosis (Chiu and Dawes, 2012). After injury, nerve tissues are under hypoxic conditions due to inflammatory reactions and ischemia. To assess whether injured nerves were hypoxic, Cattin et al. (2015) injected pimonidazole hydrochloride to rats (Xu et al., 2017) which can translate into immunofluorescent protein adducts detectabled in the conditions of hypoxic. The results indicated that there are numerous hypoxic cells before vascularization. It is known that the levels of reactive oxygen species in the brain increase with increasing blast pressure and injury , and immunohistochemical analysis of the brain sections analyzed demonstrated astrocytosis and cell apoptosis, confirming sustained neuronal injury response (Kabu et al., 2015). In the present study, many upregulated proteins were related to cell redox homeostasis, including prdx1, prdx2, prdx6, p4hb, and gpx1. The phosphorylation of prdx1, a major H_2O_2 scavenger and signaling regulator, is related to the accumulation of localized H_2O_2 that is involved in cell signaling (Woo et al., 2010). Additionally, similarly to the biological process of protein folding in SNs, there were many highly expressed proteins in

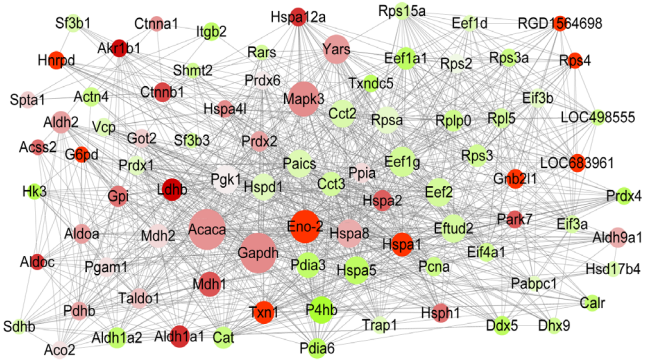

Figure 1 Identification of significantly different proteins in the SN and SI networks.
The nodes representing upregulated and downregulated proteins are shown as red and green circles, respectively. The colors of the nodes are illustrated from red to green (with white in the middle) in descending order of log2(Fold Change). The sizes of the nodes are shown from small to large in ascending order. SI: Tissues of the distal stump of the injured L2 posterior root nerve; SN: tissues of the normal L2 posterior root nerve.

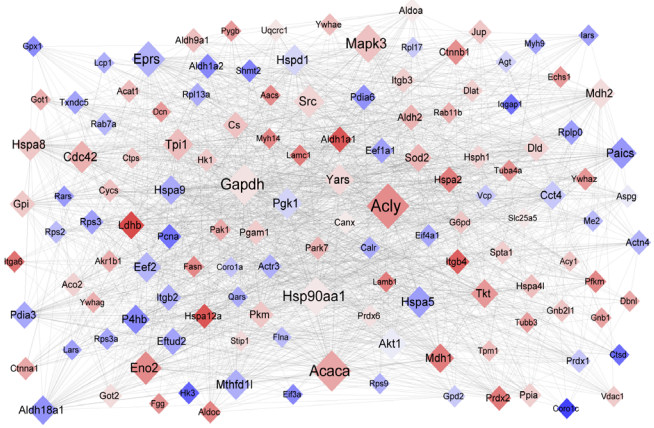

Figure 2 Identification of significantly different proteins in the MN and MI networks.
The nodes representing upregulated and downregulated proteins are shown as red and green circles, respectively. The colors of the nodes are illustrated from red to blue (with white in the middle) in descending order of log2(Fold Change). The sizes of the nodes are shown from small to large in ascending order. MI: Tissues of the proximal stump of the injured L2 anterior root nerve; MN: tissues of the normal L2 anterior root nerve.

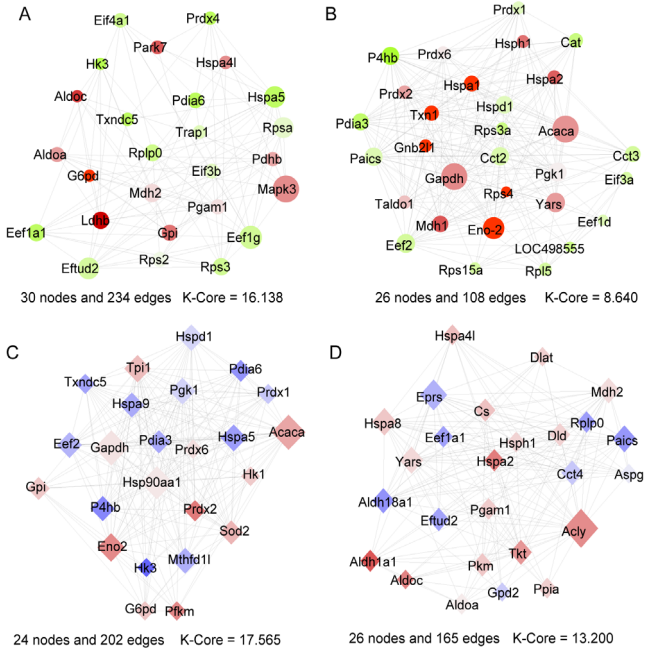

Figure 3 Sub-module analysis of the most significant nodules extracted from the giant network.
(A, B) The two most significant nodules for SN (A) and SI (B) were extracted from the giant network. Red corresponds to upregulated proteins and green corresponds to downregulated proteins. (C, D) The two most significant nodules for MN (C) and MI (D) were extracted from the giant network. Red corresponds to upregulated proteins and blue corresponds to downregulated proteins. MI: Tissues of the proximal stump of the injured L2 anterior root nerve; MN: tissues of the normal L2 anterior root nerve; SI: tissues of the distal stump of the injured L2 posterior root nerve; SN: tissues of the normal L2 posterior root nerve.

MNs, including Cct4, Hsp90aa1, Pdia3, and Pdia6. Protein folding is commonly enriched between sensory and MNs and may be a significant biological process during WD.

Common characteristics between sensory and motor nerves during Wallerian degeneration in Gene Ontology and Kyoto Encyclopedia of Genes and Genomes pathway analyses

In the GO ontology assessments of the cellular components and molecular function, the SNs and MNs appeared to have many common characteristics. The GO enrichment analysis indicated that these common genes were associated with the presence of extracellular exosomes, myelin sheath, and focal adhesion in the cellular component ontology between sensory and MNs. After nerve injury, WD begins with the degradation of the axons and myelin sheath. The most obvious characteristic of Schwann cell demyelination is that the myelin sheath decomposes into small ovoid-like structures, and the expression of the myelin gene is downregulated at the molecular level (Jessen and Mirsky, 2008). The present study observed lower expression levels of genes related to the myelin sheath in sensory and MNs, which indicates that degradation of the myelin sheath is a basic feature of WD.

Schwann cells in the peripheral nervous system release exosomes (Lopez-Verrilli and Court, 2012) and may play significant roles in neurodevelopment, neurodegeneration, and neuroprotection (Lai and Breakefield, 2012; Kalani et al., 2014). Peripheral nerve axons can internalize the exosomes released by Schwann cells, which have a positive impact on neurite outgrowth *in vitro* (Lopez-Verrilli et al., 2013). The present study also confirmed the existence of extracellular exosomes during WD, which implies that Schwann cell exosomes and their genetic cargo likely represent a vital component in the processes of WD and nerve regeneration in both sensory and MNs.

It is a little-known process that growth cone adhesion to

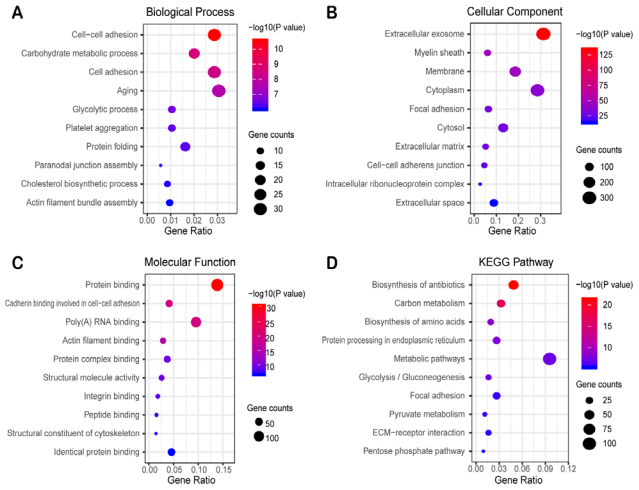

Figure 4 Enrichment analysis of 87 genes from the SN and SI networks.

(A) A bubble plot of the enriched biological process terms in the SN and SI networks. (B) A bubble plot of the enriched cellular component terms in the SN and SI networks. (C) A bubble plot of the enriched molecular function terms in the SN and SI networks. (D) A bubble plot of the enriched KEGG pathway terms in the SN and SI networks. The colors of the nodes are illustrated from red to green in descending order of –log10 (*P*-value). The sizes of the nodes are illustrated from small to large in ascending order of gene counts. The horizontal axis represents the generation, and the vertical axis represents the GO or KEGG terms. GO: Gene Ontology; KEGG: Kyoto Encyclopedia of Genes and Genomes; SI: tissues of the distal stump of the injured L2 posterior root nerve; SN: tissues of the normal L2 posterior root nerve.

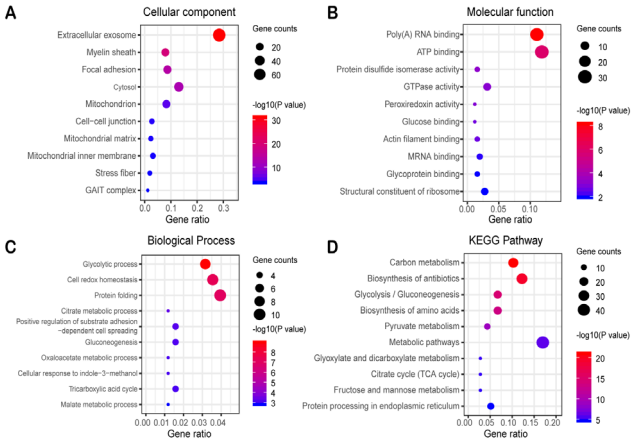

Figure 5 Enrichment analysis of 131 genes from the MN and MI network.

(A) Bubble plot of the enriched cellular component terms in the MN and MI networks. (B) Bubble plot of the enriched molecular function terms in the MN and MI networks. (C) Bubble plot of the enriched biological process terms in the MN and MI networks. (D) Bubble plot of the enriched KEGG pathway terms in the MN and MI networks. The colors of the nodes are illustrated from red to green in descending order of –log10 (*P*-value). The sizes of the nodes are illustrated from small to large in ascending order of gene counts. The horizontal axis represents the generation, and the vertical axis represents the GO or KEGG terms. GO: Gene Ontology; KEGG: Kyoto Encyclopedia of Genes and Genomes; MI: tissues of the proximal stump of the injured L2 anterior root nerve; MN: tissues of the normal L2 anterior root nerve.

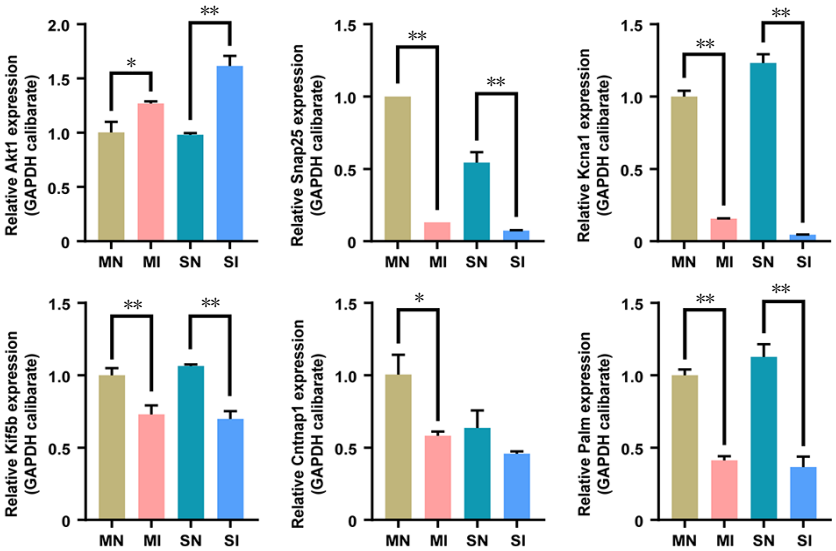

Figure 6 The expression of key genes in SN, MN, SI and MI tissues detected by quantitative real-time polymerase chain reaction.

The data are shown as the mean ± SD (n = 7, repeat independently three times). $*P < 0.05$, $**P < 0.01$ (two-sample t-test). MI: Tissues of the proximal stump of the injured L2 anterior root nerve; MN: tissues of the normal L2 anterior root nerve; SI: tissues of the distal stump of the injured L2 posterior root nerve; SN: Tissues of the normal L2 posterior root nerve.

extracellular matrix proteins at specific sites called point contacts (Renaudin et al., 1999). Point contacts come into being by growth cones in the microenvironment of nerve regeneration, which are composed of several key focal adhesion-related molecules, such as focal adhesion kinase (FAK), integrins, paxillin, and vinculin (Robles and Gomez, 2006). (Myers and Gomez, 2011) found that the control of adhesion mediated by FAK is essential for axon steering, which shows that the regulation of point contacts play an important role in the process of axon guidance. The present study also identified additional genes related to focal adhesion in sensory and MNs, including *Myh9*, *Calr*, *Rps3*, and *Actr3*. Baeyens et al. (2011) found that non-physiological metabolism of EBP50 harms myosin IIa fibers that are encoded by the *Myh9* gene, which results in decrease of focal adhesion formation. During cell migration, similarly to axon elongation, the assembly and disassembly of integrin-based focal adhesions is necessary, and can connect the actin cytoskeleton (encoded by the *Actr3* gene) to the extracellular matrix (Ridley et al., 2003). These findings suggest that regenerating axons may exist in the later stages of WD.

Additionally, our KEGG enrichment analysis indicated

that these common genes participated in carbon metabolism, metabolic pathways, protein processing in the ER biosynthesis of amino acids, and the biosynthesis of antibiotics during WD in both sensory and MNs. It is widely accepted that disturbances in nucleotide metabolism, ATP synthesis, and related purinergic signaling pathways due to injury trigger a set of cellular responses that protect the cell from virus invasion and/or homeostasis disorder (Naviaux, 2014). The type of cell damage has been labeled using a variety of terms, including the stress response of ER (Liu et al., 2008), the misfolded and unfolded protein response (Lee and Glimcher, 2009), and the oxidative stress response (Lushchak, 2011).

Key proteins in Wallerian degeneration in both sensory and motor nerves

Based on these results of GO and KEGG analysis, several genes were chosen for qRT-PCR validation, as follows: *Akt1*, *Snap25*, *Kcna1*, *Kif5b*, *Cntnap1*, and *Palm*. Importantly, the qRT-PCR results were consistent with the regulation of protein expression in iTRAQ. In the early stages of nerve injury, Schwann cells in both the proximal stump and throughout the nerve downstream of the injury dedifferentiate to progenitor-like cells, which proliferate and orchestrate an inflammatory response that clears the debris and remodels the environment. At the same time, WD occurs, and myelin sheath disintegration, axonal degradation, and inflammatory cell infiltration take place at the distal end of the injured axon (Conforti et al., 2014). There were no differences in expression in the chosen genes between MI and SI samples. *Akt1*, which is associated with the cellular response to DNA damage stimuli and hypoxia, has been reported to be upregulated in both the posterior and anterior roots of the spinal nerve after injury (Luo et al., 2010). *Snap25*, *Kcna1*, *Kif5b*, *Cntnap1*, and *Palm*, which are associated with the biological processes of axonogenesis, neuron differentiation, maintenance of membrane potential, nerve signaling, and axon guidance, have been reported to be downregulated in both the posterior and anterior roots of the spinal nerve after injury (Poliak et al., 1999; Sidor-Kaczmarek et al., 2004; Kutzleb et al., 2007; Ishida et al., 2012; Sun et al., 2013).

While different protein expression patterns in rat spinal nerves have been studied previously (He et al., 2012), protein expression patterns before and after WD have rarely been investigated. Because the spinal cord belongs to the central nervous system and the spinal nerve belongs to the peripheral nerve, which is very close to the central nervous system in anatomy. Thus, the spinal nerve may be disturbed by the central nervous system, which is one limitation of this experiment. It's still not totally clear what this limitation is, exactly, or how it might have affected the results. WD is an important component of the regeneration process after peripheral nerve injury. While it promotes nerve regeneration, it can also lead to the impairment of nerve function. However, the molecular mechanisms underlying WD are still unclear. Therefore, on the basis of the results of this study, we are in the process of further exploring the aspects of functional and pathway for the related proteins.

In summary, the present study screened DEPs that may potentially reveal differences and similarities between SNs and MNs during WD. The present findings could provide a reference point for a future investigation into the differences between sensory and motor nerves in Wallerian degeneration and the characteristics of peripheral nerve regeneration.

Acknowledgments: *We are very grateful to Xun Sun, MD, from Department of of Orthopedics, Tianjin Hospital, China, for his selfless academic guidance in the process of polishing up the manuscript and Qian Hu, Master, from Shihezi University, China, for her great moral encouragement.*

Author contributions: *Study design and paper drafting: SW, XZL, QH; experimental guidance and manuscript revision: WSW, WJX, JP, QYG, SYL; data collection and analysis: XQC, WJ, XD, GHH, PL; study methods selection of and technical support: CHS, YW. All authors read and approved the final manuscript.*

Conflicts of interest: *The authors declare that there is no conflict of interests regarding the publication of this paper.*

Financial support: *This study was supported by National Key Research & Development Program of China, No. 2016YFC11011601, 2017YFA0104701, the Youth Cultivation Project of Military Medical Science, China, No. 15QNP091 (to YW), and People's Liberation Army Youth Training Project for Medical Science of China, No. 16QNP144 (to YW). The funding bodies played no role in the study design, in the collection, analysis and interpretation of data, in the writing of the paper, or in the decision to submit the paper for publication.*

Institutional review board statement: *This study was approved by the Institutional Animal Care and Use Committee of the Chinese PLA General Hospital (Approval No. 2016-x9-07) in September 2016.*

Data sharing statement: *Datasets analyzed during the current study are available from the corresponding author on reasonable request.*

Plagiarism check: *Checked twice by iThenticate.*

Peer review: *Externally peer reviewed.*

Additional files:

Additional Figure 1: *The totally different proteins in the SN, SI, MN, and MI groups that were up- and downregulated are shown in a heatmap.*

Additional Figure 2: *The distribution of unique peptides shows a two-coordinate distribution curve of the number of unique peptides found in all proteins screened in this experiment.*

Additional Figure 3: *The peptide length distribution shows the length distribution of the peptides detected by this mass spectrometer.*

References

Abdullah M, O'Daly A, Vyas A, Rohde C, Brushart TM (2013) Adult motor axons preferentially reinnervate predegenerated muscle nerve. Exp Neurol 249:1-7.

Baeyens N, de Meester C, Yerna X, Morel N (2011) EBP50 is involved in the regulation of vascular smooth muscle cell migration and cytokinesis. J Cell Biochem 112:2574-2584.

Becker M, Nothwang HG, Friauf E (2008) Different protein profiles in inferior colliculus and cerebellum: a comparative proteomic study. Neuroscience 154:233-244.

Bittner GD, Sengelaub DR, Ghergherehchi CL (2018) Conundrums and confusions regarding how polyethylene glycol-fusion produces excellent behavioral recovery after peripheral nerve injuries. Neural Regen Res 13:53-57.

Bradford MM (1976) A rapid and sensitive method for the quantitation of microgram quantities of protein utilizing the principle of protein-dye binding. Anal Biochem 72:248-254.

Brushart TM (1988) Preferential reinnervation of motor nerves by regenerating motor axons. J Neurosci 8:1026-1031.

Cai BB, Francis J, Brin MF, Broide RS (2017) Botulinum neurotoxin type A-cleaved SNAP25 is confined to primary motor neurons and localized on the plasma membrane following intramuscular toxin injection. Neuroscience 352:155-169.

Caillaud M, Richard L, Vallat JM, Desmoulière A, Billet F (2019) Peripheral nerve regeneration and intraneural revascularization. Neural Regen Res 14:24-33.

Cattin AL, Burden JJ, Van Emmenis L, Mackenzie FE, Hoving JJ, Garcia Calavia N, Guo Y, McLaughlin M, Rosenberg LH, Quereda V, Jamecna D, Napoli I, Parrinello S, Enver T, Ruhrberg C, Lloyd AC (2015) Macrophage-induced blood vessels guide schwann cell-mediated regeneration of peripheral nerves. Cell 162:1127-1139.

Chang B, Quan Q, Sun M, Liu RX, Wang Y, Lu SB, Peng J (2017) Wallerian degeneration after peripheral nerve injury: research advance in nerve conduits. Zhongguo Zuzhi Gongcheng Yanjiu 21:1596-1603.

Chiu J, Dawes IW (2012) Redox control of cell proliferation. Trends Cell Biol 22:592-601.

Cobianchi S, de Cruz J, Navarro X (2014) Assessment of sensory thresholds and nociceptive fiber growth after sciatic nerve injury reveals the differential contribution of collateral reinnervation and nerve regeneration to neuropathic pain. Exp Neurol 255:1-11.

Conforti L, Gilley J, Coleman MP (2014) Wallerian degeneration: an emerging axon death pathway linking injury and disease. Nat Rev Neurosci 15:394-409.

Ding T, Zhu C, Yin JB, Zhang T, Lu YC, Ren J, Li YQ (2015) Slow-releasing rapamycin-coated bionic peripheral nerve scaffold promotes the regeneration of rat sciatic nerve after injury. Life Sci 122:92-99.

Franz CK, Rutishauser U, Rafuse VF (2005) Polysialylated neural cell adhesion molecule is necessary for selective targeting of regenerating motor neurons. J Neurosci 25:2081-2091.

Franz CK, Rutishauser U, Rafuse VF (2008) Intrinsic neuronal properties control selective targeting of regenerating motoneurons. Brain 131:1492-1505.

Han GH, Peng J, Liu P, Ding X, Wei S, Lu S, Wang Y (2019) Therapeutic strategies for peripheral nerve injury: decellularized nerve conduits and Schwann cell transplantation. Neural Regen Res 14:1343-1351.

Halary S, Leigh JW, Cheaib B, Lopez P, Bapteste E (2010) Network analyses structure genetic diversity in independent genetic worlds. Proc Natl Acad Sci U S A 107:127-132.

He Q, Man L, Ji Y, Zhang S, Jiang M, Ding F, Gu X (2012) Comparative proteomic analysis of differentially expressed proteins between peripheral sensory and motor nerves. J Proteome Res 11:3077-3089.

Hu Y, Park KK, Yang L, Wei X, Yang Q, Cho KS, Thielen P, Lee AH, Cartoni R, Glimcher LH, Chen DF, He Z (2012) Differential effects of unfolded protein response pathways on axon injury-induced death of retinal ganglion cells. Neuron 73:445-452.

Huang da W, Sherman BT, Lempicki RA (2009) Systematic and integrative analysis of large gene lists using DAVID bioinformatics resources. Nat Protoc 4:44-57.

Ishida S, Sakamoto Y, Nishio T, Baulac S, Kuwamura M, Ohno Y, Takizawa A, Kaneko S, Serikawa T, Mashimo T (2012) Kcna1-mutant rats dominantly display myokymia, neuromyotonia and spontaneous epileptic seizures. Brain Res 1435:154-166.

Jessen KR, Mirsky R (2008) Negative regulation of myelination: relevance for development, injury, and demyelinating disease. Glia 56:1552-1565.

Kabu S, Jaffer H, Petro M, Dudzinski D, Stewart D, Courtney A, Courtney M, Labhasetwar V (2015) Blast-associated shock waves result in increased brain vascular leakage and elevated ROS levels in a rat model of traumatic brain injury. PLoS One 10:e0127971.

Kalani A, Tyagi A, Tyagi N (2014) Exosomes: mediators of neurodegeneration, neuroprotection and therapeutics. Mol Neurobiol 49:590-600.

Karegar M, Mohammadi R (2015) Assessment of neuroregenerative effect of dihydrotestosterone, on peripheral nerve regeneration using allografts: a rat sciatic nerve model. Neurol Res 37:908-915.

Kearns G, Wang S (2012) Medical diagnosis of cubital tunnel syndrome ameliorated with thrust manipulation of the elbow and carpals. J Man Manip Ther 20:90-95.

Kutzleb C, Petrasch-Parwez E, Kilimann MW (2007) Cellular and subcellular localization of paralemmin-1, a protein involved in cell shape control, in the rat brain, adrenal gland and kidney. Histochem Cell Biol 127:13-30.

Kwon YW, Masutani H, Nakamura H, Ishii Y, Yodoi J (2003) Redox regulation of cell growth and cell death. Biol Chem 384:991-996.

López-Barea J, Gómez-Ariza JL (2006) Environmental proteomics and metallomics. Proteomics 6:S51-S62.

Lai CP, Breakefield XO (2012) Role of exosomes/microvesicles in the nervous system and use in emerging therapies. Front Physiol 3:228.

Langley JN, Anderson HK (1904) The union of different kinds of nerve fibres. J Physiol 31:365-391.

Lee AH, Glimcher LH (2009) Intersection of the unfolded protein response and hepatic lipid metabolism. Cell Mol Life Sci 66:2835-2850.

Lim TK, Shi XQ, Johnson JM, Rone MB, Antel JP, David S, Zhang J (2015) Peripheral nerve injury induces persistent vascular dysfunction and endoneurial hypoxia, contributing to the genesis of neuropathic pain. J Neurosci 35:3346-3359.

Liu G, Sun Y, Li Z, Song T, Wang H, Zhang Y, Ge Z (2008) Apoptosis induced by endoplasmic reticulum stress involved in diabetic kidney disease. Biochem Biophys Res Commun 370:651-656.

Lopez-Verrilli MA, Court FA (2012) Transfer of vesicles from schwann cells to axons: a novel mechanism of communication in the peripheral nervous system. Front Physiol 3:205.

Lopez-Verrilli MA, Picou F, Court FA (2013) Schwann cell-derived exosomes enhance axonal regeneration in the peripheral nervous system. Glia 61:1795-1806.

Lu A, Wiśniewski JR, Mann M (2009) Comparative proteomic profiling of membrane proteins in rat cerebellum, spinal cord, and sciatic nerve. J Proteome Res 8:2418-2425.

Luo C, Yi B, Bai L, Xia Y, Wang G, Qian G, Feng H (2010) Suppression of Akt1 phosphorylation by adenoviral transfer of the PTEN gene inhibits hypoxia-induced proliferation of rat pulmonary arterial smooth muscle cells. Biochem Biophys Res Commun 397:486-492.

Lushchak VI (2011) Adaptive response to oxidative stress: Bacteria, fungi, plants and animals. Comp Biochem Physiol C Toxicol Pharmacol 153:175-190.

Miller EK, Raese JD, Morrison-Bogorad M (1991) Expression of heat shock protein 70 and heat shock cognate 70 messenger RNAs in rat cortex and cerebellum after heat shock or amphetamine treatment. J Neurochem 56:2060-2071.

Murakawa H, Togashi H (2015) Continuous models for cell-cell adhesion. J Theor Biol 374:1-12.

Myers JP, Gomez TM (2011) Focal adhesion kinase promotes integrin adhesion dynamics necessary for chemotropic turning of nerve growth cones. J Neurosci 31:13585-13595.

Namgung U (2014) The role of Schwann cell-axon interaction in peripheral nerve regeneration. Cells Tissues Organs 200:6-12.

Naviaux RK (2014) Metabolic features of the cell danger response. Mitochondrion 16:7-17.

Pereira JA, Lebrun-Julien F, Suter U (2012) Molecular mechanisms regulating myelination in the peripheral nervous system. Trends Neurosci 35:123-134.

Poliak S, Gollan L, Martinez R, Custer A, Einheber S, Salzer JL, Trimmer JS, Shrager P, Peles E (1999) Caspr2, a new member of the neurexin superfamily, is localized at the juxtaparanodes of myelinated axons and associates with K^+ channels. Neuron 24:1037-1047.

Raivich G, Kreutzberg GW (1993) Peripheral nerve regeneration: role of growth factors and their receptors. Int J Dev Neurosci 11:311-324.

Ramon y Cajal S (1928) Degeneration and regeneration of the nervous system. Oxford, England: Clarendon Press.

Renaudin A, Lehmann M, Girault J, McKerracher L (1999) Organization of point contacts in neuronal growth cones. J Neurosci Res 55:458-471.

Ridley AJ, Schwartz MA, Burridge K, Firtel RA, Ginsberg MH, Borisy G, Parsons JT, Horwitz AR (2003) Cell migration: integrating signals from front to back. Science 302:1704-1709.

Robles E, Gomez TM (2006) Focal adhesion kinase signaling at sites of integrin-mediated adhesion controls axon pathfinding. Nat Neurosci 9:1274-1283.

Ron D, Walter P (2007) Signal integration in the endoplasmic reticulum unfolded protein response. Nat Rev Mol Cell Biol 8:519-529.

Sidor-Kaczmarek J, Labuda C, Litwinowicz B, Spodnik JH, Kowianski P, Dziewiatkowski J, Morys J (2004) Developmental expression of SNAP-25 protein in the rat striatum and cerebral cortex. Folia Morphol (Warsz) 63:285-288.

Sun T, Yu N, Zhai LK, Li N, Zhang C, Zhou L, Huang Z, Jiang XY, Shen Y, Chen ZY (2013) c-Jun NH2-terminal kinase (JNK)-interacting protein-3 (JIP3) regulates neuronal axon elongation in a kinesin- and JNK-dependent manner. J Biol Chem 288:14531-14543.

Unwin RD, Griffiths JR, Whetton AD (2010) Simultaneous analysis of relative protein expression levels across multiple samples using iTRAQ isobaric tags with 2D nano LC-MS/MS. Nat Protoc 5:1574-1582.

Woo HA, Yim SH, Shin DH, Kang D, Yu DY, Rhee SG (2010) Inactivation of peroxiredoxin I by phosphorylation allows localized H(2)O(2) accumulation for cell signaling. Cell 140:517-528.

Xiong L, Zhang B, Shen RW, Ji AY, Sun GQ, Bian HL, Zhang FY, Wang Y, Huang H, Li HQ, Zhou SY, Shen ZK, Wang Z (2016) Toll-like receptor 4 antagonist protects against Wallerian degeneration after peripheral nerve injury. Zhongguo Zuzhi Gongcheng Yanjiu 20:6308-6316.

Xu X, Zhu Q, Zhang R, Wang Y, Niu F, Wang W, Sun D, Wang A (2017) ITRAQ-Based Proteomics Analysis of Acute Lung Injury Induced by Oleic Acid in Mice. Cell Physiol Biochem 44:1949-1964.

Zhang P, Zhu S, Li Y, Zhao M, Liu M, Gao J, Ding S, Li J (2016) Quantitative proteomics analysis to identify diffuse axonal injury biomarkers in rats using iTRAQ coupled LC-MS/MS. J Proteomics 133:93-99.

Zhang Y, Li Z, Yang M, Wang D, Yu L, Guo C, Guo X, Lin N (2013) Identification of GRB2 and GAB1 coexpression as an unfavorable prognostic factor for hepatocellular carcinoma by a combination of expression profile and network analysis. PLoS One 8:e85170.

C-Editor: Zhao M; S-Editors: Yu J, Li CH; L-Editors: Cason N, Yu J, Song LP; T-Editor: Jia Y

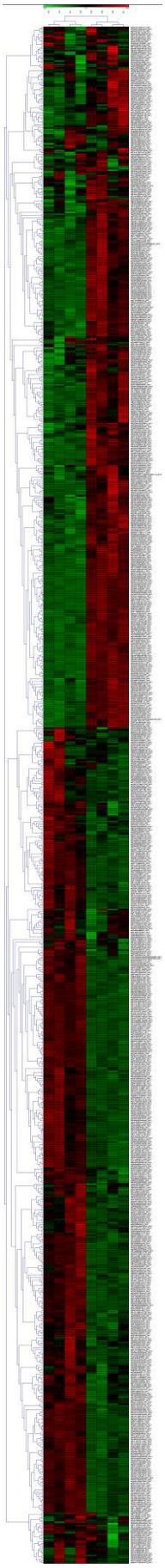

Additional Figure 1 The totally different proteins in the SN, SI, MN, and MI groups that were up- and downregulated are shown in a heatmap. Red represents up-regulated protein and green represents down-regulated protein.

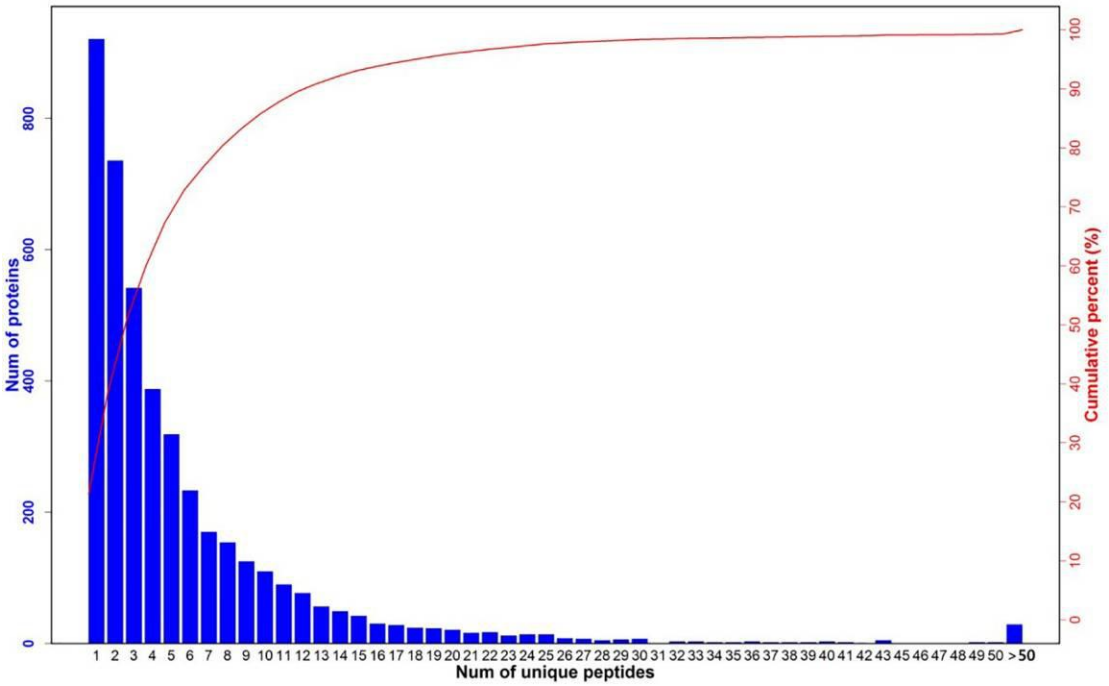

Additional Figure 2 The distribution of unique peptides shows a two-coordinate distribution curve of the number of unique peptides found in all proteins screened in this experiment.

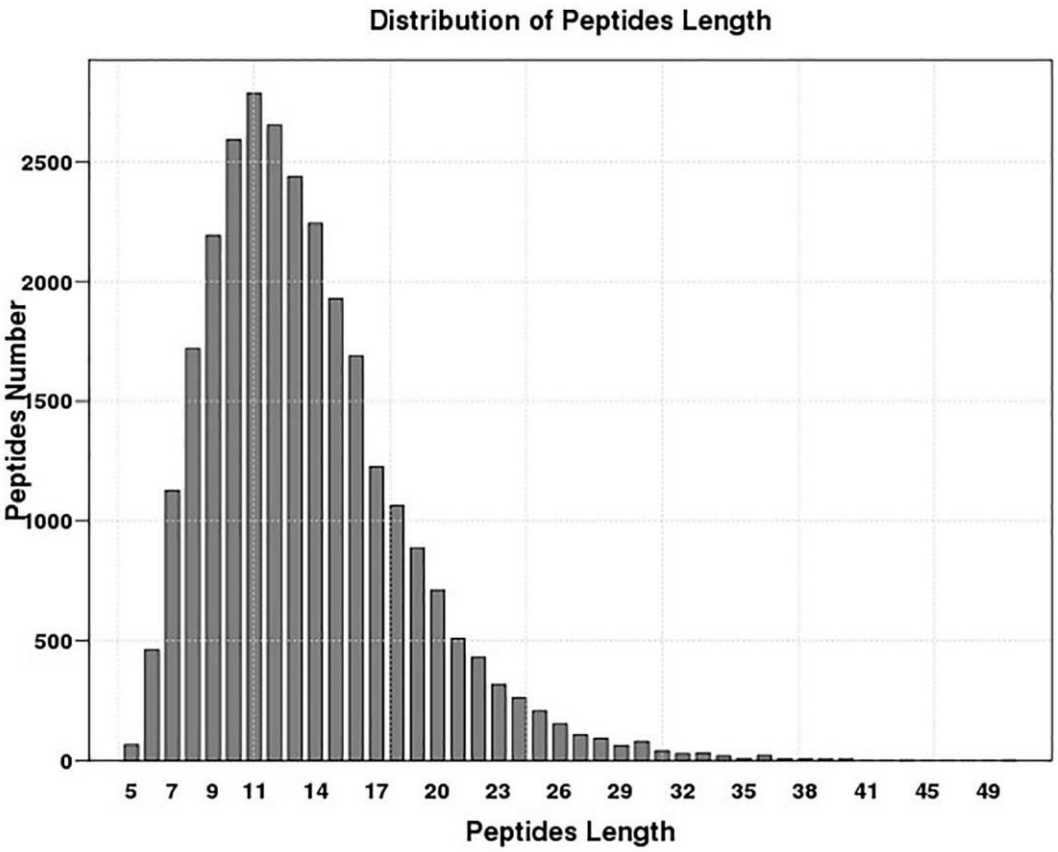

Additional Figure 3 The peptide length distribution shows the length distribution of the peptides detected by this mass spectrometer.